# Al-ions effect on structural, optical, antibacterial, and photocatalytic activities of ZnO nanostructures

Z. Ullah[a], M. T. Qureshi[b,*], K. Sultana[a], F. Ullah[c], A. Khalid[a], N. Masood[d], F. I.A. Abdella[d], S. A. Elhag[e]
[a]*Department of Physics, Hazara University Mansehra, 21300 Khyber Pakhtunkhwa Pakistan*
[b]*Basic Science Department, College of Preparatory Year, University of Ha'il, Ha'il 1560, Saudi Arabia*
[c]*Departement of Physics and Biophysics, University of warmia and Mazury, Olsztyn, Poland*
[d]*Department of Chemistry, Faculty of Science, University of Ha'il, Ha'il, Saudi Arabia*
[e]*Department of Chemistry, University of Bahri, Khartoum, Sudan*

In this work, Pure and aluminum doped zinc oxide nanostructures were successfully synthesized through a well-established hydrothermal method. The hexagonal wurtzite structure, and nano porous shape for Al dopant in ZnO were confirmed via XRD and SEM analysis. The reduction in energy band gap (3.40 to 3.19 eV) for Al dopant samples and enhancement in inhibition zones (7 mm- 17 mm) for pure and Al-doped ZnO were recorded. The photocatalytic activity of Al doped ZnO was shown to be several times more efficient than in prior studies. The enhancement in these parameters suggest that these materials are good candidates for biomedical and optoelectronic applications.

(Received April 24, 2023; Accepted August 15, 2023)

*Keywords:* ZnO nanostructured, X-rays diffraction, Band gap, Antimicrobial activity.

## 1. Introduction

Nanotechnology has evolved into an efficient technology with a wide range of applications. Nanosized have been shown to improved surface morphology for a variety of biomedical applications, along with antibacterial activity, environmental clean-up, tissue engineering, drug delivery, etc [1]. Zinc oxide (ZnO) is an n-type semiconductor with bandgap (Eg) energy of 3.37 eV and a higher binding energy than other semiconductors (60 meV), due to such distinctive properties as low price, large amount in nature, non-toxicity, suitability to doping [2]. Semiconductors have a wide range of applications including Photocatalysis, thin-film transistors, nonlinear optics, and gas transistors are illustrations of optical and electrical applications for solar energy conversion. Sensors, pigments, cosmetics, LEDs, UV and low radiation sensors, photo luminescent sensor and textiles [3]. In addition, ZnO has a good UV response in this region and great electron transport properties. ZnO not only has virtually zero toxicity but is also a biocompatible oxide. Suitable material or use in internal biological implants, biosensors, as well as medium and bimolecular sensors for drug delivery [4-6].

UV radiation having a wavelength of 385 nm or less can be absorbed by ZnO. However, as visible light contributes for 45 percent of solar radiation energy (SRE) and UV light accounts for a smaller amount less than 10%, photo catalysts like ZnO should absorb not only UV but visible light also for better photocatalytic efficiency and various practical uses. The band gap (Eg) of ZnO must be constricted or split into numerous sub-gaps in absorbing visible light, accomplished by placing transition metal ions. Microbial infections are major problem in the healthcare and food industry, but antimicrobial agents and surface coatings have become

* Corresponding authors: tauseefqureshi1981@gmail.com
https://doi.org/10.15251/DJNB.2023.183.995

widespread in recent years [7]. Several researchers have tried to add transition metal ions to the ZnO lattice to improve the antibacterial function of ZnO. Metal oxide nanostructure (MON) has been extensively analyzed to determine their ability as an antibacterial agent. The production of nanoparticles on bacteria's surfaces, as well as their development in the cytoplasm and periplasm, causes cellular disruption [8]. Hydrothermal method has many advantages over other preparation such as reactive thermal evaporation. [9], electro spray method [10], sol–gel [11], solvent casting method [12], chemical bath deposition (CBD) [13], salvo-thermal process [14], rf-magnetron sputtering [15], co precipitation method [16], and pulsed laser deposition [17]. In this study, Al doped ZnO nanostructures with various Al concentrations (0, 10, 15, 20 at. %) were prepared using the hydrothermal method. Further it has examined the effect of pure and aluminum-doped ZnO-Ns on the band gap and gram-negative bacteria (P. aeruginosa). We observed the band gap of nanoparticles reduced (Eg) and enhanced the inhibition zone of gram-negative bacterial strains by the Al-doped ZnO-NS.

## 2. Experimental details

### 2.1. Materials and methods

Pure ZnO and Aluminum doped ZnO nanostructures with different concentration ($Al_xZn_xO_{1-x}$, where x=10% wt., 15% wt., 20% wt.) were prepared using well-known hydrothermal approach [18]. Zinc Chloride ($ZnCl_2$) and Aluminum chloride hexahydrate ($AlCl_3.6H_2O$) used as precursors for the preparation of samples. $ZnCl_2$ (3.4g) dissolved in 50 mL distilled water under steady stirring. The 0.47g of hexamethylenetetramine (HMTA) was also diffused into 30ml of deionized water and poured into prepared solution drop wise under vigorous stirring at room temperature for 40 minutes. For doping, three different ratios of Al (10%wt, 15%wt, 20%wt) were added along with $ZnCl_2$. The resulting solution was shifted in an autoclave and kept in oven for 14 hours at 150°C. The obtained product was then allowed to cool down to room temperature, centrifuged, and filtered several times with D.I water and ethanol. The pure and doped solutions were both handled in the same way; this duration was determined by prior studies and was chosen to maintain excellent crystalline nature. Finally, the structures were dried at 100$^o$C, and ready for further use.

The crystalline nature of ZnO and Al:ZnO samples were evaluated with X-ray diffractometer (JDX-3532) and Morphological features were analysed through scanning electron microscope (JEOL JSM-6460LV). Chemical composition was determined through energy dispersive X-ray spectroscopy and absorption spectrum was obtained using UV-visible spectrometer (Shimadzu UV-1600). Antibacterial activity of ZnO and Al:ZnO nanopowders with various concentrations of stock solution were tested using Pseudomonas aeruginosa (gram-negative) bacterial strains. Initially, 500 ml distilled water was stirred in 9.5 grams Muller Hinton. The resulting product was placed in the autoclave, and the reaction temperature (121°C) was maintained for 15 minutes before placing 25 ml into each plate. With the use of cork bores, create a 6mm well using the well diffusion method. Then, pour 100 volumes of bacterial strain onto a plate and establish a colony, as well as 50µl of zinc oxide into each well incubate each well at 370°C for 24 hours.

Under UV light irradiation, the photocatalytic activities of ZnO and AZO nanostructures were tested utilizing methyl orange (MO) degradation in aqueous solution (1000W, main wave crest at 365 nm). To produce adsorption/desorption equilibration, 30 mg of photo catalysts were combined with 42 mL of MO aqueous solution (200 mg/L) in a quartz beaker to form a suspended solution, which was then ultrasound dispersed for 30 minutes. From the beaker, 4 mL of suspensions were removed. After then, the suspension was subjected to UV light. In 10 minute, intervals, 4 mL of suspensions were removed from the beaker. To separate the suspended solid, each suspension was centrifuged right away. The band maximum (466 nm) in the absorption spectra of these suspensions was then used to calculate the MO concentrations.

## 3. Results and discussion

### 3.1. X-rays diffraction Analysis

The X-ray diffraction pattern of synthesized for pure and aluminum doped zinc oxide nanostructures are shown in figure 1. In the XRD spectrum, the peaks observed at 31.6°, 34.3°, 36.1°, 47.4°, 56.4°, 62.7°, and 67.8°. These peaks can be linked to the hexagonal wurtzite structure (JCPDS: 01-079-0207) of zinc oxide correspond to planes (100), (002), (101), (102), (110), (103), and (112) and the lattice parameters (a=b=3.2568 nm and c=5.2125 nm). When the concentration of dopant was increased, the FWHM (full with half maxima) increased, and the peaks shifted to somewhat higher angles. Because aluminum has a smaller ionic radius then zinc and oxygen, this phenomenon is explained by Bragg's rule, which states that dopants produce a decrease in the interplanar distance. The effects of crystal size can be attributed to the broadening of the peaks exhibited in the X-ray diffraction pattern of the manufactured samples.

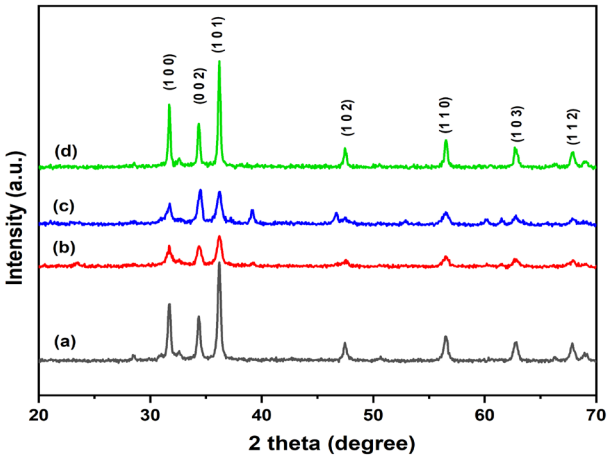


*Fig. 1. X-ray diffraction patterns of powder samples (a) pure ZnO, (b) 10 wt.% (c) 15 wt.% and (d) 20 wt.% Al doped.*

The sharper peaks not only indicate that the particles are smaller, but they also reflect the effects of the experimental conditions on crystalline nuclei nucleation and growth. This also indicates the quantum confinement of the particles. The highest intensity for (101) reflection is found in pure ZnO nanostructures, indicating that the particles (grains) are predominantly orientated along the c-axis. This is due to the low internal stress and surface energy, as well as the high atomic density, which allows crystallites to develop easily along the c-axis. For 20 wt. % Al doping, the intensity of (101) reflection increases [18]. It's happened due to the lower surface energy caused by the substitution of Al at Zn sites, the preferential orientation along the (101) plane is more pronounced. The addition of Al, the intensities of diffraction peaks reduced (broadening), indicating a loss of crystallinity and an increase in the surface defect content of the samples. Extra defects and distorted lattice structures arise as the concentration of Al doped increases. As a result, the Al doped ZnO nanostructures material has larger grain sizes and shapes than the undoped sample. However, as the doping level is increased, the crystallite size decreases, eventually reaching 7.04 nm for 20 at% Al-doped ZnO nanostructures. This was due to the hydrothermal process's lower sintering rate. The pure and aluminum doped Zinc Oxide (ZnO) nanostructures having average crystallite size was calculated using the Debye-Scherer formula

$$D = 0.9\lambda/\beta \cos\theta \quad (1)$$

where $D$ is the crystallite size in nanometers (nm), $\lambda$ is the wavelength of incident X-ray (nm), $\beta$ is the full width at half maximum, and $\theta$ is the diffraction angle. Table 1 shows the tabulation of the crystallite size, lattice constants (a and c values), unit cell volume, c/a ratio, and dislocation

density. When the c/a ratio was kept constant, a decrease was observed in the cell volume and the lattice parameter of the nanostructure.

The extent of defects in the sample is determined by the dislocation density, i.e., larger the dislocation density, higher the hardness. Increased dopant concentrations resulted in a rise in the extent of defects and the nanostructure's dislocation density (δ). This is caused by the Al ions of the ZnO lattice being replaced by a material with a lower valance band [19-23]. The obtained values are very close to those that have been published previously. We can therefore conclusively state that the addition of aluminum affects the structure of the ZnO significantly.

### 3.2. Morphological studies

Scanning electron microscopy (SEM) was used to determine the shape of the material as shown in figure 2. These micro porous structures have demonstrated the development of ZnO and AZO nanostructures. The Al concentration increased then agglomeration increased [24], the particle size of zinc oxide (ZnO) treated with aluminum reduced significantly due to varying of doping concentrations [25]. Pure ZnO nanostructure have grains like shape evenly spread across the whole surface of the substrate, resulting in a granular surface, whereas ZnO doped with 10% Al have light glassy structures, with a 15% of Al doping, the particles grains of nanostructure are granular and spherical. Similarly with further 20% increase in Al content, the particle has a porous nature and lacks a close-packed shape, which is advantageous for photovoltaic and high potential for sensors applications [26-27].

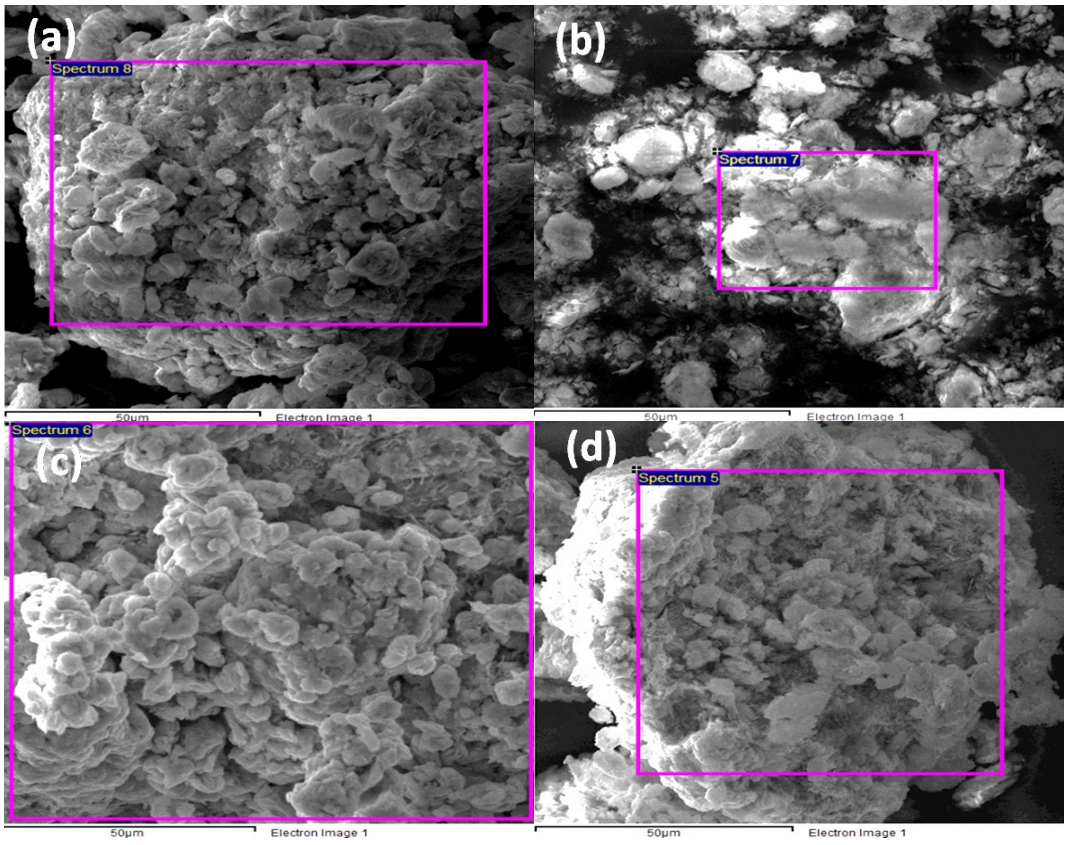


*Fig. 2. SEM micrographs for (a) pure ZnO,(b) 10wt %, (c) 15 wt.% and (d) 20 wt.% of Al doped ZnO nanostructures.*

### 3.3. EDX analysis

Energy dispersive X-ray spectroscopy was used to confirm the chemical composition of the samples. Figure 3 shows the EDX spectra of a pure ZnO, 10 wt.%, 15 wt.%, and 20 wt.% Al doped ZnO, indicating that undoped ZnO and Al doped ZnO nanostructure were synthesized. This

indicates that Al has been successful in his doping efforts. Sharp signals for zinc and oxygen were observed in undoped ZnO nano structure confirming the growth of ZnO nano structure, also a very small amount 0.22 by wt% are present in pure ZnO arise due to the aluminum foil. However, some chlorine signals were observed, their percentage has been negligible. This could happen during the synthesis of a chemical reaction involving the extract that was used to prepare the samples. Peaks and percentage composition of EDX for all the prepared samples fabricated through hydrothermal method are shown in table 2.

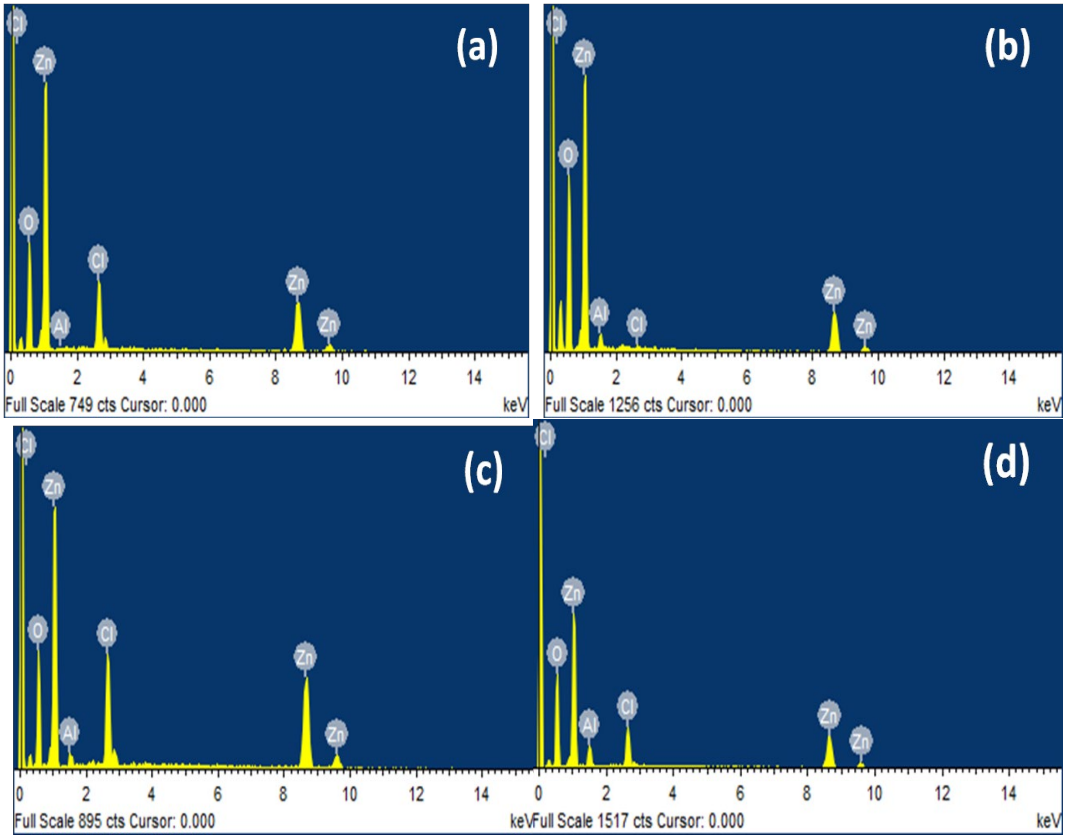


*Fig. 3. EDX spectra of (a) pure ZnO, (b) 10 wt. %, (c) 15wt%., and (d) 20wt.% Al-doped ZnO NPs.*

*Table 2. Quantitative analysis of samples by weight % for elements Zn, O and Al.*

| Elements | Pure ZnO | 10wt% Al:ZnO | 15wt% Al:ZnO | 20wt% Al:ZnO |
|---|---|---|---|---|
| Zn | 55.99 | 49.65 | 62.13 | 47.60 |
| O | 33.70 | 46.86 | 24.99 | 39.16 |
| Al | 0.22 | 2.87 | 1.48 | 5.18 |
| Cl | 10.09 | 0.62 | 11.40 | 8.06 |
| 100.00 | 100.00 | 100.00 | 100.00 | 100.00 |

### 3.4. Optical properties

Optical properties of pure and Al doped ZnO were studied by obtaining the absorbance spectra in the UV-visible range as well as by calculating the band gap value through Tauc plot method as shown in figure 4. Figure 4(a) designates the absorption spectra of pure and aluminum doped zinc oxide measured between 200 and 600 nm. The bandgap coefficient develops in the range 200–260 nm depending on the concentration of the solution, which indicates that with an increase in the concentration of the doping material, aluminum ions in $Zn^{+2}$ ion, the absorption edge of the spectra changes towards longer wavelengths, higher energy (blue shift) [28], this blue

shift can be attributed to the agglomerations in the samples. The direct transition of electrons in ZnO nano crystals blue shift of the absorption edge can be explained. The band gap (Eg) can be obtained from the absorption coefficient, which can be calculated as a function of the photon energy.

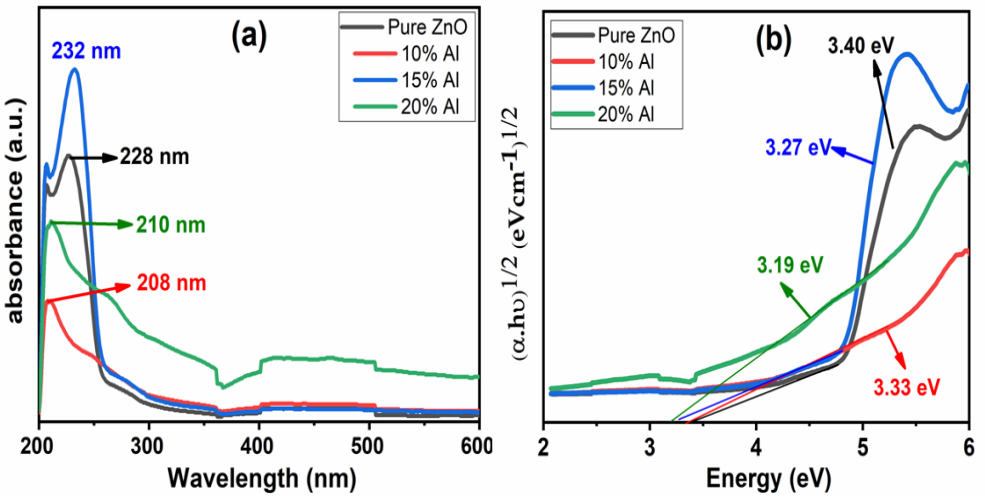


*Fig. 4. UV-Vis spectroscopy curves here (a) Absorbance spectra and (b): Tauc-plot for pure ZnO and Al doped ZnO nanostructures.*

The band gap of pure and Al-doped ZnO was calculated by using Tauc-Davis and Mott relation given by.

$$(\alpha h\nu)^{1/2} = A(h\nu - Eg) \quad (2)$$

where α, ν, A and Eg are absorption coefficient, light frequency, proportionality constant and band gap, respectively as shown in figure 4(b). The calculated values of the energy for forbidden zone are varies from 3.46 to 3.19 eV depending on the concentration of the Aluminum solution from 0% to 20% are in good agreement with the indicated values [29-30]. The inclusion of Al in a ZnO nanostructure induces lattice damage or structural defects that generate defect energy levels below the conduction band (CB), resulting decrease in the forbidden energy of the nanostructure, since lattice defects are proportional to the Al concentration. Therefore, the energy gap (Eg) gradually decreases with an increase in the Al content in ZnO nanoporous structure.

*Table 3. Band gap values of pure ZnO and, 10%, 15%, and 20% Al-doped ZnO.*

| Samples | Band gaps |
|---|---|
| ZnO | 3.40 eV |
| 10%Al | 3.33 eV |
| 15%Al | 3.27 eV |
| 20%Al | 3.19 eV |

### 3.5. Determination of antimicrobial activity

Pseudomonas aeruginosa is a frequent nosocomial bacterium that causes high-mortality infections. Hyper-mutable (or mutator) P. aeruginosa, which has a high genetic variation, is found in a variety of chronic diseases, including lung infections in cystic fibrosis patients (CF). As a result, new plans for the development and approval of unique manufacturing agents against these bacterial species are extremely desirable. The antibacterial activity of zinc oxide (ZnO) and

aluminum doped zinc oxide (Al:ZnO) was investigated in different amounts of Pseudomonas aeruginosa bacterial strains, and the zones of inhibition of these samples were measured as shown in figure 5. When the quantity of Al doping in the samples was raised, the antibacterial characteristics of the samples were observed to improve [31]. It can be observed from figure 5(d) that increasing the Al doping level up to 20 wt% which improves the antibacterial activity of Al: ZnO nano powders, which might be due to the formation of a greater number of free electrons generated by the substitutional assimilation of Al ions.

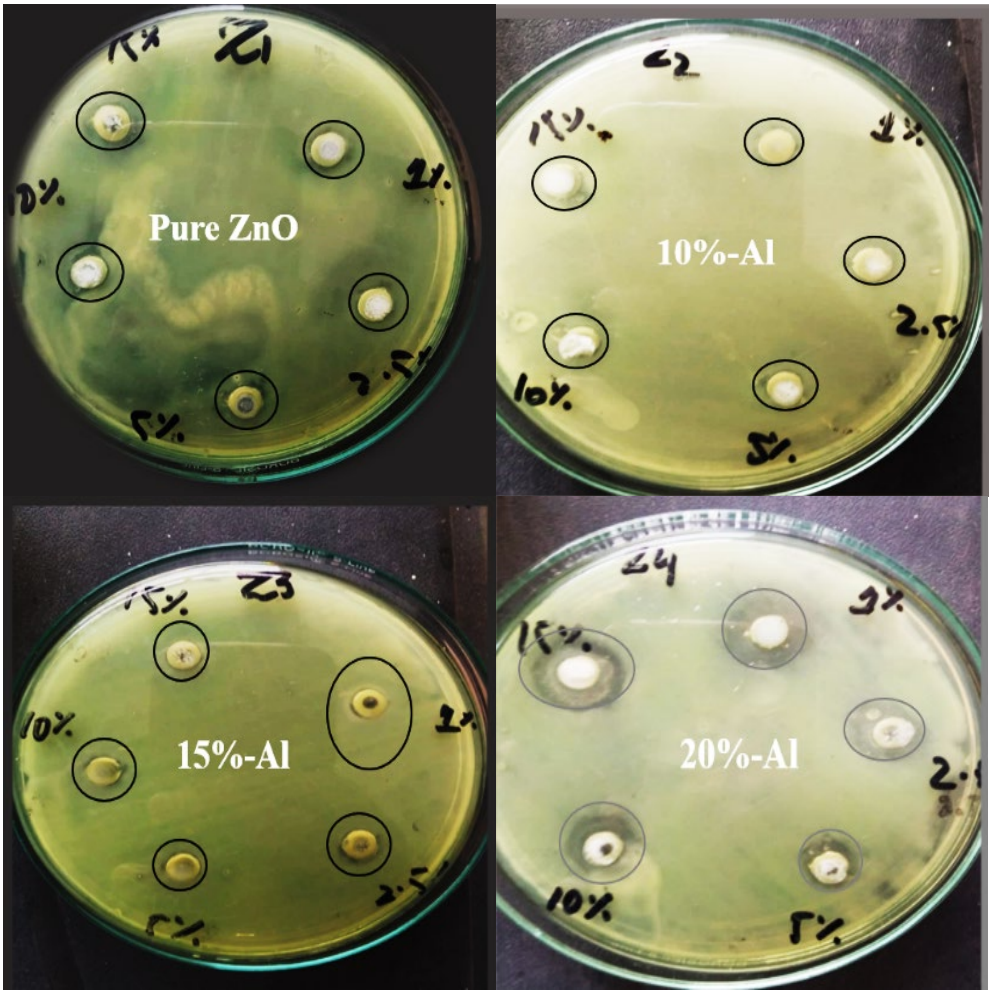


*Fig. 5. Zone of inhibition against P. aeruginosa bacteria where (Z1)shows Pure ZnO, (Z2), (Z3) and (Z4) represents 10 wt.%, 15 wt.% and 20 wt.% Al doped ZnO respectively.*

Pairs of electrons and holes play a very vital role in the production of reactive oxygen species (ROS). Amongst ROS, $H_2O_2$ is a dominant oxidizing agent; it penetrates directly into the cell membrane of bacteria, causes different kinds of damage, and inhibits cell growth, although negative charge hydroxyl radicals and superoxide anions cannot enter the cell membrane, these cause significant damage to proteins, lipids, DNA, and the outer wall components of bacteria [32 33]. As a result, bacteria will be destroyed. The antibacterial activity of the samples is linked to the generation of reactive oxygen species (ROS), particularly hydroxyl free radicals ($OH^-$), when they are exposed to ultraviolet light. Oxidative stress is caused by the creation of reactive oxygen species (ROS), that causes DNA damage and cell death [34]. The released $Zn2^+$-ions can enter into the cell membrane, destroying the cell wall and causing cell content leakage. The diffusion of $Zn^{2+}$ ions from ZnO nanostructure into food, drinking water, and other materials will not harm humans because Zn is a good nutrient.

Figure 5 shows the rate of inhibition of Gram-negative bacteria culture growth in the existence of ZnO and Al-ZnO nanostructures, ZnO NS steadily decreased the development of the bacterial culture after doping with aluminum. The antibacterial properties of the preparations are affected by a variety of parameters including pH, size, ionic strength, and capping agent. Doping with aluminum oxide caused a sharp decrease in bacterial growth, while the degree of inhibition depended on the concentration (1%, 2.5%, 5%, 10%, and 15%).

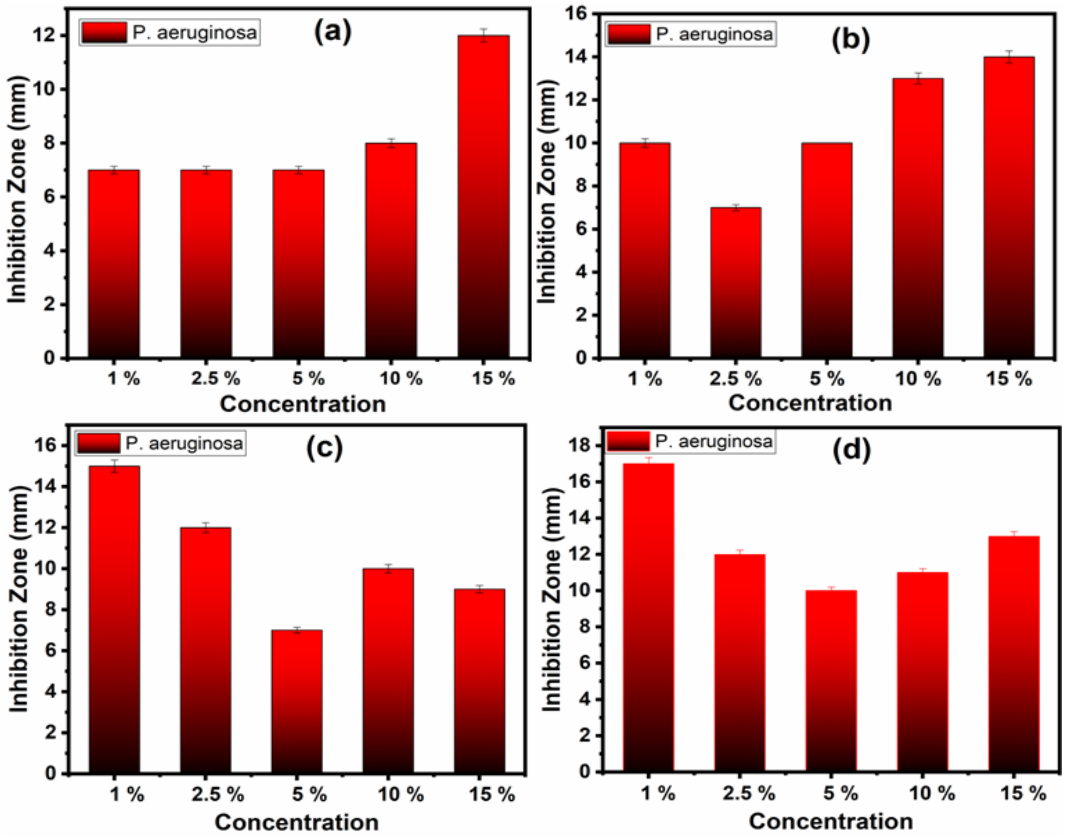


*Fig. 6. Growth inhibition of P. aeruginosa by (a) Pure ZnO, (b) 10 wt.%, (c) 15wt.%, and (d) 20wt.% Al doped ZnO.*

The inhibition zone in P. aeruginosa is different for pure and aluminum doped zinc oxide as shown by bar graphs in figure 6. The zone of inhibition for pure ZnO solution and Al doped ZnO compositions (1-15% solution concentration) increased from 7-17 mm as shown Fig. 6(a-d). Aluminum Zinc Oxide has a unique antibacterial property against Gram-negative bacteria (GNB), as indicated by the efficiency of ZnO and Al:ZnO Ns in inhibiting P. aeruginosa growth **[35-36].** The nanostructures activity may be caused in two stages: first, by causing damage to the bacterial cell wall's outer membrane through direct interaction or electrostatic with the materials; second, oxidative stress is created by establishing an active oxygen environment.

### 3.6. Photocatalytic activity

The photocatalytic activities of the samples were assessed by detecting the degradation of methyl orange in an aqueous solution when UV light was irradiated. Photo-excitation of the photo catalyst surface with UV-Vis irradiation initiates the photocatalytic reaction, which can supply the required band gap energy to form photoactivated electron-hole pairs [39]. Photo generated holes can oxidize organic molecules to form R+ or OH-/H2O to form OH radical [40-41]. Most MO dyes can be oxidized to mineral end-products by the OH radical, which has a high oxidizing capability [42]. The photo generated electrons on the photocatalyst surface react with adsorbed

oxygen as electron acceptors, which is critical for lowering the electron-hole pair recombination rate. The recombination of electrons and holes on the photo-catalyst surface has a detrimental impact on reduction and oxidation reactions, diminishing the effective interactions and, as a result, the performance.

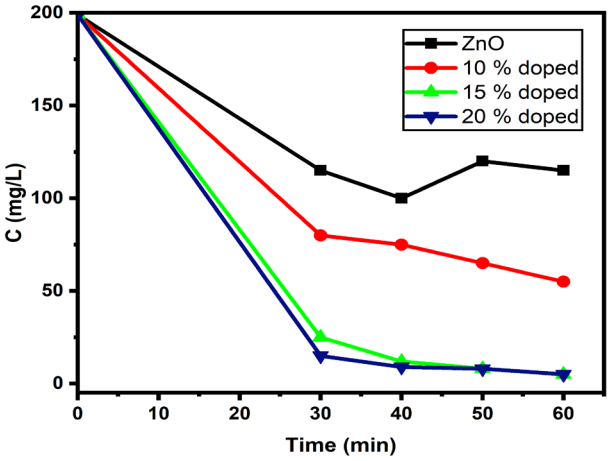


*Fig. 7. The photocatalytic activity of pure and Al doped ZnO nanostructured under UV light.*

Figure 7 depicts the results and shows that with the addition of Al, the absorption capacities and photocatalytic activity rise. The absorption action could explain the modest increase in MO content after 50 minutes for pure ZnO. The nanostructure containing 20 wt.% Al has unrivalled absorption ability, lowering MO concentration from 200 to 2.7 mg/L and photo degrading MO completely within 30 minutes of irradiation. The photo stability of 20 wt% doped was also demonstrated. This dominating photocatalytic activity is thought to be related to a slower charge recombination rate produced by the presence of Al, as well as a larger surface area caused by the smaller particle size [43]. The 15 wt.% doped and 20 wt.% doped curves are slightly separated, indicating that the absorption capacity and photocatalytic activity have reached saturation. When the doping content reaches a certain level, the superfluous Al is thought to convert to amorphous $Al_2O_3$. Furthermore, the amount of amorphous $Al_2O_3$ increases with the amount of doping, and the presence of amorphous $Al_2O_3$ lowers Al doped ZnO homogeneity.

## 4. Conclusion

The hydrothermal approach was used for successful synthesizes of pure and Al doped ZnO nanostructures and their physical and biological properties were investigated. The XRD results shows that the crystallite size reduced when doped 20 wt.% of Al in ZnO. The absorption spectra exhibited a blue shift. This clearly indicates a shift of the bandgap (Eg) towards lower values, which was also confirmed by UV spectroscopy. The bandgap reduces from 3.40 to 3.19 eV with increasing Al concentration. Al: ZnO NSs have strong antibacterial capability against the harmful microorganisms that were tested. Antibacterial activity tests on Pseudomonas aeruginosa were used to confirm the materials' antimicrobial activity, with rise in the quantity of doping, higher antibacterial activity is observed. As a result, the use of Ns materials as bactericidal agents is motivated by their bacteriostatic properties. To put it another way, the effect of ZnO NSs on bacteria is demons treated by their direct interaction, which alters the permeability of the outer membrane, produces intracellular oxidative stress, restricts cell development, and eventually leads to bacterial death. The characteristics of the produced nano powders indicate that they have a lot of potential for variety technological applications. Under visible light illumination, 20% doped sample has the maximum photocatalytic efficiency.

The Al doped ZnO samples with high concentrations had outstanding photocatalytic and adsorption capabilities. Nanostructures containing 20% Al have already demonstrated exceptional absorption ability, lowering MO concentration from 200 to 2.7 mg/L and photo degrading MO completely within 30 minutes of irradiation which finally recomemmded that these materials can be used as a suitable dose against bacterial diseases.

**Acknowledgements**

The Authors would like to thank Scientific Research Deanship at Ha'il University-Saudi Arabia for financial support of this project through Project Number RG-20119.

## References

[1] V. Saxena, LM.Pandey, Materials Today Proceedings, Vol. 18, pp. 1388-400, 2019; https://doi.org/10.1016/j.matpr.2019.06.605

[2] W. Khan, ZA Khan, AA Saad, S Shervani, A Saleem , AH Naqvi, International Journal of Modern Physics, World Scientific Publishing Company, Vol. 22, pp. 630-636, Conference Series 2013; https://doi.org/10.1142/S2010194513010775

[3] A. Alkahlout, N Al Dahoudi, I Grobelsek, M Jilavi, journal of Materials, 2014; https://doi.org/10.1155/2014/235638

[4] G. Murillo, E Leon-Salguero, PR Martínez-Alanis, J Esteve, J Alvarado-Rivera, F Güell, Nano Energy Vol. 60, pp. 817-26, 2019; https://doi.org/10.1016/j.nanoen.2019.04.017

[5] MD Tyona, Zinc Oxide Based Nano Materials and Devices, London, United Kingdom Intech Open, Sep 5 2019; https://doi.org/10.5772/intechopen.86254

[6] S Zhang, Y Li, G Sun, B Zhang, Y Wang, J Cao, Z Zhang, Applied Surface Science, Vol. 497, pp. 143811, 2019; https://doi.org/10.1016/j.apsusc.2019.143811

[7] MG Nair, M Nirmala, K Rekha, A Anukaliani, Materials Letters, Vol. 65, No12 pp. 1797-800, 2011; https://doi.org/10.1016/j.matlet.2011.03.079

[8] S Getie, A Belay, AR Chandra Reddy, Z Belay, J Nanomed Nanotechno S, Vol. 8, pp. 004, 2017; https://doi.org/10.4172/2157-7439.S8-004

[9] FK Mugwang'a, PK Karimi, WK Njoroge, O Omayio, J Fundam Renewable Energy Appl, Vol. 5, No.170, pp.2, 2015; https://doi.org/10.4172/2090-4541.1000170

[10] G Marinov, K Lovchinov, V Madjarova, V Strijkova, M Vasileva, N Malinowski, T Babeva, Optical Materials, Vol. 1, pp. 89-390, 2019; https://doi.org/10.1016/j.optmat.2019.01.055

[11] M Ali, S Sharif, S Anjum, M Imran, M Ikram, M Naz, S Ali, Materials Research Express, Vol. 6, No. 12, pp.1250 d5, 2020; https://doi.org/10.1088/2053-1591/ab6383

[12] IS Elashmawi, NA Hakeem, LK Marei, FF Hanna, Physica B Condensed Matter, Vol. 405, No19, pp. 4163-9, 2010; https://doi.org/10.1016/j.physb.2010.07.006

[13] R Chandramohan, TA Vijayan, S Arumugam, HB Ramalingam, V Dhanasekaran, K Sundaram, T Mahalingam, Materials Science and Engineering, B, Vol. 176,No.2, pp.152-6, 2011; https://doi.org/10.1016/j.mseb.2010.10.017

[14] Y Liu, H Liu, Z Chen, N Kadasala, C Mao, Y Wang, Y Zhang, H Liu, Y Liu, J Yang, Y Yan, Journal of alloys and compounds, Vol. 604, pp. 281-5, 2014; https://doi.org/10.1016/j.jallcom.2014.03.079

[15] Z Zhang, C Bao, W Yao, S Ma, L Zhang, S Hou, Superlattices and Microstructures, Vol. 49, No. 6, pp. 644-53, 2011; https://doi.org/10.1016/j.spmi.2011.04.002

[16] PS Sundaram, T Sangeetha, S Rajakarthihan, R Vijayalaksmi, A Elangovan, G Arivazhagan, Physica B: Condensed Matter, Vol. 595, pp. 412342, 2020; https://doi.org/10.1016/j.physb.2020.412342

[17] AM Mostafa, EA Mwafy, NS Awwad, HA Ibrahium, Radiation Physics and Chemistry, Vol.

179, pp.109233, 2021; https://doi.org/10.1016/j.radphyschem.2020.109233

[18] A Ullah, AM Toufiq, MT Qureshi, A Khan, M Younas, ST Obeidat, MA Elaimi, RA Hameed, F Ullah, Digest Journal of Nanomaterials and Biostructures, Vol. 17,No. 3, pp. 949-960, 2022; https://doi.org/10.15251/DJNB.2022.173.949

[19] A Khan, R Hussain, AM Toufiq, A Shah, BA Khan, Z Niaz, S ur Rahman, Materials Characterization, Vol. 169, pp. 110661, 2020; https://doi.org/10.1016/j.matchar.2020.110661

[20] Z Aghagoli, M Ardyanian, Journal of Materials Science, Materials in Electronics, Vol. 29, No. 9, pp. 7130-41, 2018; https://doi.org/10.1007/s10854-018-8701-4

[21] A Narjis, H El Aakib, M Boukendil, M El Hasnaoui, L Nkhaili, A Aberkouks, A Outzourhit, Journal of King Saud University-Science, Vol. 32 (1): pp.1074-80, 2020; https://doi.org/10.1016/j.jksus.2019.10.004

[22] M Sajjad, I Ullah, MI Khan, J Khan, MY Khan, MT Qureshi, Results in Physics, Vol.1, No. 9, pp.1301-9, 2018; https://doi.org/10.1016/j.rinp.2018.04.010

[23] MR Bindhu, K Ancy, M Umadevi, GA Esmail, NA Al-Dhabi, MV Arasu, Journal of Photochemistry and Photobiology B Biology, Vol. 210, pp. 111965, 2020; https://doi.org/10.1016/j.jphotobiol.2020.111965

[24] W Khan, ZA Khan, AA Saad, S Shervani, A Saleem, AH Naqvi, Conference Series World Scientific Publishing Company, Vol. 22, pp. 630-636, 2013; https://doi.org/10.1142/S2010194513010775

[25] M Oves, M Arshad, MS Khan, AS Ahmed, A Azam, IM Ismail, Targeting water borne bacteria, Journal of Saudi Chemical Society, Vol. 19, No 5, pp.581-8, 2015; https://doi.org/10.1016/j.jscs.2015.05.003

[26] NJ Ridha, FK Alosfur, MH Jumali, S Radiman, Nanotechnology, Vol. 16, No. 31(14), pp.145502, 2020; https://doi.org/10.1088/1361-6528/ab6235

[27] C Manoharan, G Pavithra, M Bououdina, S Dhanapandian, P Dhamodharan, Applied Nanoscience, Vol. 6, No. 6, pp.815-25, 2016; https://doi.org/10.1007/s13204-015-0493-8

[28] R Jayakrishnan, K Mohanachandran, R Sreekumar, CS Kartha, KP Vijayakumar, Materials science in semiconductor processing, Vol.16, No.2, pp.326-31, 2013; https://doi.org/10.1016/j.mssp.2012.10.003

[29] FK Shan, BI Kim, GX Liu, ZF Liu, JY Sohn, WJ Lee, BC Shin, YS Yu, Journal of Applied Physics, Vol. 95, No.9, pp. 4772-6, 2004; https://doi.org/10.1063/1.1690091

[30] A Chanda, S Gupta, M Vasundhara, SR Joshi, GR Mutta, J Singh, RSC advances, Vol. 7, No. 80, pp.50527-36, 2017; https://doi.org/10.1039/C7RA08458G

[31] K Ravichandran, P Sathish, S Snega, K Karthika, PV Rajkumar, K Subha, B Sakthivel, Powder Technology, Vol. 274, pp. 250-7, 2015; https://doi.org/10.1016/j.powtec.2014.12.053

[32] M Vasanthi, K Ravichandran, NJ Begum, G Muruganantham, S Snega, A Panneerselvam, P Kavitha, Superlattices and Microstructures, Vol. 55, pp. 180-90, 2013; https://doi.org/10.1016/j.spmi.2012.12.011

[33] S Snega, K Ravichandran, N Jabena Begum, K Thirumurugan, Journal of Materials Science, Materials in Electronics, Vol. 24, No. 1, pp. 135-41, 2013; https://doi.org/10.1007/s10854-012-0956-6

[34] PP Fu, Q Xia, HM Hwang, PC Ray, H Yu, Journal of food and drug analysis, Vol. 1, No. 22 (1), pp. 64-75 2014; https://doi.org/10.1016/j.jfda.2014.01.005

[35] SC Esparza-González, S Sánchez-Valdés, SN Ramírez-Barrón, MJ Loera-Arias, J Bernal, HI Meléndez-Ortiz, R Betancourt-Galindo, Toxicology In Vitro, Vol. 37, pp.134-41, 2016; https://doi.org/10.1016/j.tiv.2016.09.020

[36] KS Khashan, GM Sulaiman, SA Hussain, TR Marzoog, MS Jabir, Journal of Inorganic and Organometallic Polymers and Materials, Vol. 30 (9), pp. 3677-93, 2020; https://doi.org/10.1007/s10904-020-01522-9

[37] UG Akpan, BH Hameed, Journal of hazardous materials, Vol. 170 (2-3) pp. 520-9, 2009; https://doi.org/10.1016/j.jhazmat.2009.05.039

[38] D Li, Q Zhu, C Han, Y Yang, W Jiang, Z Zhang, Journal of Hazardous Materials, Vol. 285 pp. 398-408, 2015; https://doi.org/10.1016/j.jhazmat.2014.12.024

[39] R Wahab, F Khan, RB Singh, NK Kaushik, J Ahmad, MA Siddiqui, Q Saquib, BA Ali, ST Khan, J Musarrat, AA Al-Khedhairy, Physica E: Low-dimensional Systems and Nanostructures, Vol. 69, pp. 101-8, 2015; https://doi.org/10.1016/j.physe.2015.01.005

[40] A Khalid, P Ahmad, AI Alharth, S Muhammad, MU Khandaker, MR Faruque, IU Din, MA Alotaibi, Materials Research Express, Vol. 9, No. 8(4), pp. 045006 2021; https://doi.org/10.1088/2053-1591/abf2e9

[41] Z Razzaq, A Khalid, P Ahmad, M Farooq, MU Khandaker, A Sulieman, IU Rehman, S Shakeel, A Khan, Catalysts, Vol. 11(6): pp.709, 2021; https://doi.org/10.3390/catal11060709

[42] M Ahmad, E Ahmed, Y Zhang, NR Khalid, J Xu, M Ullah, Z Hong, Current Applied Physics,; Vol. 13(4), pp. 697-704, 2013; https://doi.org/10.1016/j.cap.2012.11.008